Strong shear softening induced by superionic hydrogen in Earth's inner core

Wenzhong Wang[1,2,3,*], Yunguo Li[1,4,5], John P. Brodholt[1,6], Lidunka Vočadlo[1], Michael J. Walter[2], Zhongqing Wu[3,5,7]

[1]Department of Earth Sciences, University College London, London WC1E 6BT, United Kingdom

[2]Earth and Planets Laboratory, Carnegie Institution for Science, Washington, DC 20015, USA

[3]Laboratory of Seismology and Physics of Earth's Interior, School of Earth and Space Sciences, University of Science and Technology of China, Hefei, Anhui 230026, China

[4]CAS Key Laboratory of Crust–Mantle Materials and Environments, School of Earth and Space Sciences, University of Science and Technology of China, Hefei, Anhui 230026, China

[5]CAS Center for Excellence in Comparative Planetology, USTC, Hefei, Anhui 230026, China

[6]Centre for Earth Evolution and Dynamics, University of Oslo, Oslo, Norway

[7]National Geophysical Observatory at Mengcheng, USTC, Hefei, Anhui 230026, China

*Correspondence to: Wenzhong Wang (wenzhong.wang@ucl.ac.uk)

Abstract

Geophysical and geochemical evidence suggests that Earth's core is predominantly made of iron (or iron-nickel alloy) with several percent of light elements. However, Earth's solid inner core transmits shear waves at a much lower velocity than expected from mineralogical models that are consistent with geochemical constraints. Here we investigate the effect of hydrogen on the elastic properties of iron and iron-silicon alloys using *ab initio* molecular dynamic simulations. We find that these H-bearing alloys maintain a superionic state under inner-core conditions and that their shear moduli exhibit a strong shear softening due to the superionic effect, with a corresponding reduction in V_S. Several *hcp*-iron-silicon-hydrogen compositions can explain the observed density, V_P, V_S, and Poisson's ratio of the inner core simultaneously. Our results indicate that hydrogen is a significant component of the Earth's core, and that it may contain at least four ocean masses of water. This indicates that the Earth may have accreted wet and obtained its water from chondritic and/or nebular materials before or during core formation.

Keywords: superionic Fe alloy, shear softening, Earth's core, low shear velocity, high Poisson's ratio, *ab initio* molecular simulations

1. Introduction

Earth's core plays a fundamental role in the evolution and habitability of our planet (Rubie et al., 2015). It is responsible for the geodynamo and hence for the generation of Earth's magnetic field (Glatzmaier and Roberts, 1996, 1995). It also records important information regarding the history of Earth's accretion (Wood et al., 2006) and influences the subsequent evolution of the mantle, crust, and atmosphere (Nimmo, 2015). Earth's core consists of a liquid outer core and a solid inner core that are both predominantly composed of iron (Fe) with about 5-15 wt% nickel (Ni). However, seismological observations demonstrate that the core density is 3-10% lower than that expected for the molten/solid iron-nickel alloy (Alfè et al., 2000; Anderson and Ahrens, 1994; Birch, 1964; Ichikawa et al., 2014; Vočadlo et al., 2009), suggesting the presence of a substantial amount of less dense, or "light" elements in the core (Badro et al., 2014; Huang et al., 2019; Kawaguchi et al., 2017; Li and Fei, 2014; Mao et al., 2012). Light elements that have been proposed include silicon (Si), sulfur (S), carbon (C), oxygen (O), and hydrogen (H) (Poirier, 1994), but in what combination and concentrations is unknown.

Information about Earth's core is obtained from seismology and chemical models must be consistent with seismic observations. One of the most intriguing characteristics revealed by seismic studies is that Earth's inner core transmits shear waves at anomalously low velocity (V_S=~3.6 km/s) (Dziewonski and Anderson, 1981; Kennett et al., 1995), which results in a high Poisson's ratio (ν=~0.44). Although significant effort has been devoted to investigating the velocities and/or densities of binary Fe or Fe-Ni alloys with light elements (Antonangeli et al., 2010; Bazhanova et al., 2012; Huang et al., 2019; Mao et al., 2012; Martorell et al., 2013a; Tagawa et al., 2016; Vočadlo, 2007), none have yet explained the low V_S, the high Poisson's ratio, and the density of the inner core simultaneously. A high-pressure phase of iron carbide, Fe_7C_3, was reported to have a low V_S and high Poisson's ratio similar to those of the Earth's inner core due to elastic softening prior to melting (Chen et al., 2014; Li et al., 2016;

Prescher et al., 2015), but its density is ~8% lower than seismic models and thus cannot be the main phase of the inner core (Li et al., 2016). Hexagonal close-packed iron (*hcp*-Fe) was found to show a strong pre-melting shear softening that can explain the observed velocities (Martorell et al., 2013b), but pure *hcp*-Fe has a higher density and light elements are required. However, the incorporation of light elements will suppress the pre-melting softening, and inversely, increase the sound velocities (Martorell et al., 2016). A recent *ab initio* study found that some ternary *hcp* Fe-Si-C alloys can match the velocities and density of the inner core and C is an indispensable component (Li et al., 2018). However, only a small amount of C is expected to partition into the solid phase during the crystallization of the inner core (Li et al., 2019), rendering these composition irrelevant for the inner core, although this latter study suggested that the combined effects of multiple light elements may increase C partitioning into the inner core. And finally, the presence of a small fraction of melt was proposed to explain the observed V_S of the inner core (Singh et al., 2000; Vočadlo, 2007), but whether and how the liquid could exist in the inner core remains unknown.

The core is potentially the largest reservoir of H in the Earth's interior. Recently, Li et al. (2020) calculated the H partition coefficient between iron and silicate melts at high pressures and temperatures by combining *ab initio* molecular dynamics and thermodynamic integration and found that H prefers to partition into the iron liquid under core-formation conditions (Y. Li et al., 2020). The actual amount of H in the core depends on how much water was dissolved into the silicate mantle during core-mantle differentiation, which is related to water in the materials accreting to form Earth and its accretion processes. New measurements of enstatite chondrites (EC), which are believed to be representative, at least in part, of the materials that formed Earth (Dauphas, 2017), reveal that they can contain hydrogen at abundance levels and have hydrogen and nitrogen isotopic compositions similar to those of Earth’s mantle (Piani et al., 2020). Although the timing for the delivery of water from EC into Earth is not well constrained, the simplest model is where Earth's water originated in the nebular

material from which the planet accreted and that subsequent core formation could have segregated more than three-quarters of hydrogen into the core (Y. Li et al., 2020). Indeed, liquid Fe with about 1 wt% H can reproduce the compressional wave velocity (V_P) and density of the outer core (Umemoto and Hirose, 2015). Hydrogen would partition into solid iron with the growth of the inner core, as solid and liquid iron have a similar local environment for H (Okuchi, 1997). Consequently, a substantial amount of H likely exists in the inner core alloying with Fe.

In this work, we present *ab initio* molecular dynamic (AIMD) simulations of the elastic properties of *hcp*-Fe-H alloys under inner-core conditions. We first focus on the binary Fe-H system and extend this to the ternary Fe-Si-H system as geochemical evidence suggests substantial Si in the core (Georg et al., 2007; Shahar et al., 2009) and the Si partition coefficient between solid and liquid iron is ~1 (Alfè et al., 2002; Zhang et al., 2020). We do not consider the effect of C and O since both elements preferentially enter into the liquid outer core during the growth of the inner core (Alfè et al., 2002; Li et al., 2019; Zhang et al., 2020). In summary, we find that H is highly diffusive in the solid Fe-H and Fe-Si-H alloys under inner-core conditions and this superionic effect leads to a strong shear softening that can explain the observed velocities and density of the inner core.

2. Methods

We performed *ab initio* molecular dynamic (AIMD) simulations based on density functional theory (DFT) using VASP with the projector-augmented wave (PAW) method (Blöchl, 1994). The generalized-gradient approximation (GGA) (Perdew et al., 1996) in the PBE parameterization was used for the exchange-correlation functional together with PAW-PBE pseudopotentials. The energy cutoff was 400 eV. The K-point for Brillouin zone summations over the electronic states is 2×2×2. Single-particle orbitals were populated based on the Fermi–Dirac statistics. The time step was set to be 1 fs. We ran finite temperature Born–Oppenheimer AIMD simulations on supercells of

hcp-$Fe_{64}H_4$ (0.111 wt.%), $Fe_{60}Si_4H$ (0.029 wt.%), $Fe_{60}Si_4H_2$ (0.058 wt.%), $Fe_{60}Si_4H_4$ (0.115 wt.%), and $Fe_{60}Si_4H_8$ (0.230 wt.%), in which interstitial H atoms were randomly distributed in initial structures of *hcp*-Fe_{64} and $Fe_{60}Si_4$. The crystal structure of $Fe_{60}Si_4$ has been well investigated by Li et al. (2018) and the quasi-random structure was used in this study.

We ran NPT simulations in the isothermal-isobaric ensemble to relax the supercell at the target temperatures and pressure (360 GPa) using a Langevin thermostat (Parrinello and Rahman, 1980). These simulations were run for 10 ps to obtain the initial lattice parameters of Fe-H and Fe-Si-H alloys. We then performed NVT simulations with the Langevin thermostat for over 15 ps using the lattice parameters from NPT simulations at the target temperatures to ensure the pressure was maintained at 360 GPa and the structure remained under hydrostatic conditions within 1 GPa; if not, we manually made minor adjustments to the supercell parameters and ran the NVT simulations again until 360 GPa was achieved. Thus, we determined the final cell parameters of these alloys at different temperatures and 360 GPa.

In order to calculate the isothermal elastic constants, we applied four different strains (±0.01 and ±0.02) to the unit cells from NPT-NVT simulations and performed NVT simulations with the Langevin thermostat to obtain the stresses. The NVT simulations on the strained boxes were run for 15 ps and the stresses were averaged from the last 10 ps of the simulations. By fitting the stress-strain relationship with second-order polynomials and calculating the slopes at zero strain, we obtained the isothermal elastic constants (C_{11}, C_{33}, C_{12}, C_{13}, C_{44}, and C_{66}). The adiabatic elastic constants were derived using the following equations:

$$\begin{aligned} C_{11}^S &= C_{11}^T + \alpha\gamma T K_T \\ C_{33}^S &= C_{33}^T + \alpha\gamma T K_T \\ C_{12}^S &= C_{12}^T + \alpha\gamma T K_T \\ C_{13}^S &= C_{13}^T + \alpha\gamma T K_T \\ C_{44}^S &= C_{44}^T \end{aligned} \tag{1}$$

$$C_{66}^{S} = C_{66}^{T}$$

where α is the thermal expansion coefficient ($\alpha=1\times10^{-5}$/K) (Vočadlo, 2007; Vočadlo et al., 2003), γ is the Grüneisen parameter (γ=1.5) (Vočadlo, 2007; Vočadlo et al., 2003), K_T is the isothermal bulk modulus that was calculated from the isothermal elastic constants using the Voigt-Reuss-Hill (VRH) average (Hill, 1952). The adiabatic bulk modulus (K_S) and shear modulus (G) were obtained by using the VRH averages, and the compressional wave velocity (V_P) and shear wave velocity (V_S) are calculated from the elastic moduli and density using $V_P = \sqrt{(K_S + \frac{4}{3}G)/\rho}$ and $V_S = \sqrt{G/\rho}$. The isothermal elastic constants and bulk modulus, the adiabatic elastic moduli, and the sound velocities are listed in Table S1.

The statistical errors of the temperatures and stresses were estimated by the blocking method used in (Martorell et al., 2013b). The standard deviation is defined as:

$$\delta = \sqrt{\frac{C_0'}{n'-1}\left(1 + \frac{1}{\sqrt{2(n'-1)}}\right)} \quad (2)$$

where $n' = n/2$, $C_0' = \frac{1}{n'}\sum_{k=1}^{n'}(x_k' - \bar{x})^2$, and $x_k' = (x_{2k-1} + x_{2k})/2$, $\bar{x}$ is the average, n is the number of data points. The final temperatures were averaged from the last 10 ps of the NVT simulations and the temperature error increases from 3 K to 9 K when the target temperature increases from 2000 K to 6500 K. The errors on the elastic constants were obtained from the statistical errors of stresses and the uncertainties of the second-order polynomial fitting, and then the errors on elastic moduli and sound velocities were derived based on the rule of linear error propagation:

$$\Delta F = \sum_C \left|\left(\frac{\partial F}{\partial C}\right)\Delta C\right| \quad (3)$$

The errors associated with elastic properties and sound velocities are shown in Table S1.

3. Results and discussion

3.1 Binary *hcp*-Fe-H alloy

We start with the binary *hcp*-Fe-H alloy under different temperatures and 360 GPa.

The elastic properties and sound velocities of *hcp*-$Fe_{64}H_4$ are compared with those of *hcp*-Fe (Martorell et al., 2013b) in Fig. 1. Compared with *hcp*-Fe, the *hcp*-$Fe_{64}H_4$ alloy has lower elastic moduli and sound velocities, and except for K_S, they decrease with temperature more rapidly. For instance, when temperature increases from 2000 K to 6500 K, the G, V_P, and V_S of *hcp*-$Fe_{64}H_4$ decreases by 62.0%, 10.6%, and 37.3%, respectively, while these reductions for *hcp*-Fe are in turn about 42.6%, 7.2%, and 22.9% (Martorell et al., 2013b). As a result, the differences in G, V_P, and V_S between *hcp*-Fe and *hcp*-$Fe_{64}H_4$ increase significantly with temperature (Fig. 1). At 2000 K, G, V_P, and V_S of *hcp*-$Fe_{64}H_4$ drop by 5.8%, 1.3%, and 2.8% relative to pure Fe respectively, while these properties reduce by 37.6%, 5.0%, and 20.9% at 6500 K, respectively. By comparison, the K_S of *hcp*-$Fe_{64}H_4$ is only ~2.0% lower than that of *hcp*-Fe at 2000-6500 K.

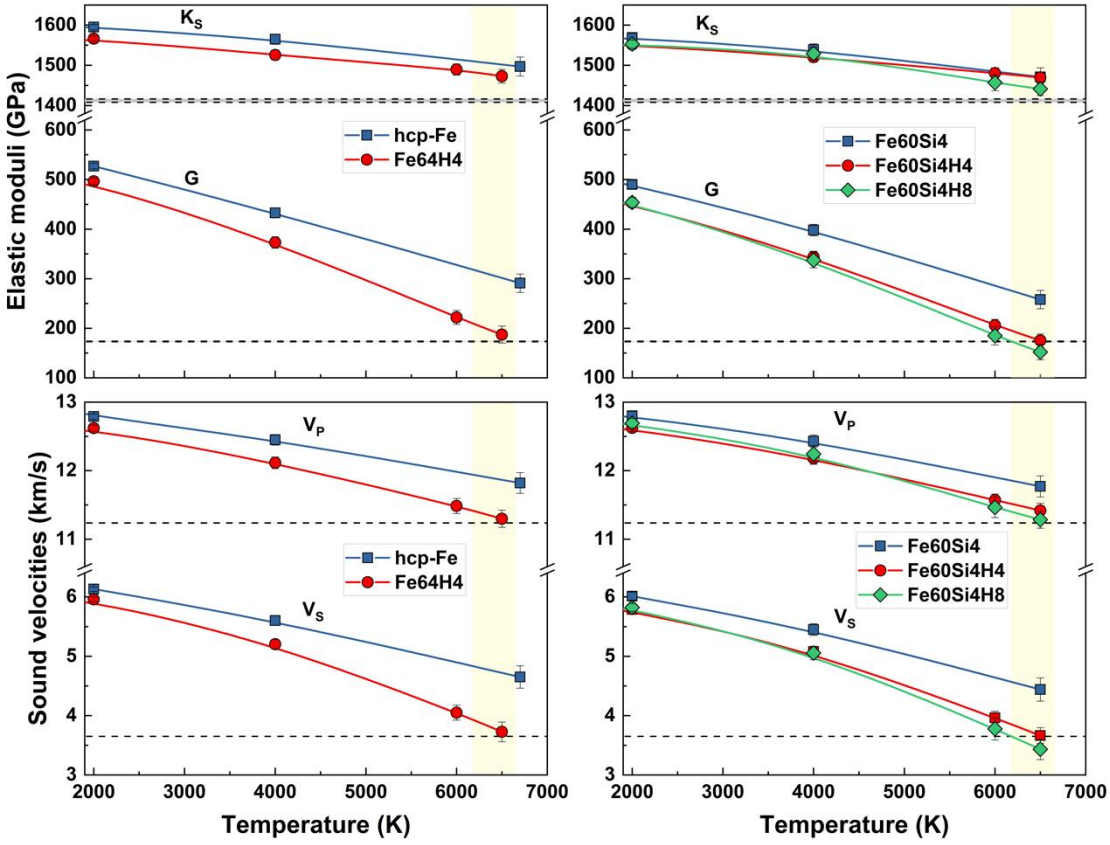

Figure 1. Elastic properties and sound velocities of H-bearing alloys as a function of temperature at 360 GPa. **Left column:** elastic moduli (K_S and G) and sound velocities (V_P and V_S) of *hcp*-$Fe_{64}H_4$ compared with those of *hcp*-Fe (Martorell et al., 2013b).

Right column: *hcp*-$Fe_{60}Si_4H_4$ and $Fe_{60}Si_4H_8$ in comparison with the *hcp*-$Fe_{60}Si_4$ (Li et al., 2018). The dash lines refer to the seismic observations from the PREM and AK135 model (Dziewonski and Anderson, 1981; Kennett et al., 1995). The yellow shaded regions represent the possible temperatures at the inner-core boundary (ICB).

It should be noted that *hcp*-$Fe_{64}H_4$ is still a solid phase at 360 GPa and even 6500 K, as revealed by the small mean-square displacements (MSDs) of Fe atoms (Fig. S1). However, the MSDs of H atoms increase monotonically with simulation time at temperatures above 4000 K (Fig. S1), becoming highly diffusive with liquid-like mobility - a "superionic state", which has some of the properties of a liquid and of a solid simultaneously (Cavazzoni et al., 1999). Superionicity was first predicted by the AIMD simulations in solid water and ammonia phases at the extreme conditions of giant-planetary interiors (Cavazzoni et al., 1999) and has been verified by recent X-ray diffraction measurements (Millot et al., 2019). The superionic H observed in *hcp*-$Fe_{64}H_4$ makes this alloy have an intermediate G between a solid and a liquid (G=0), which can explain shear softening under inner-core conditions.

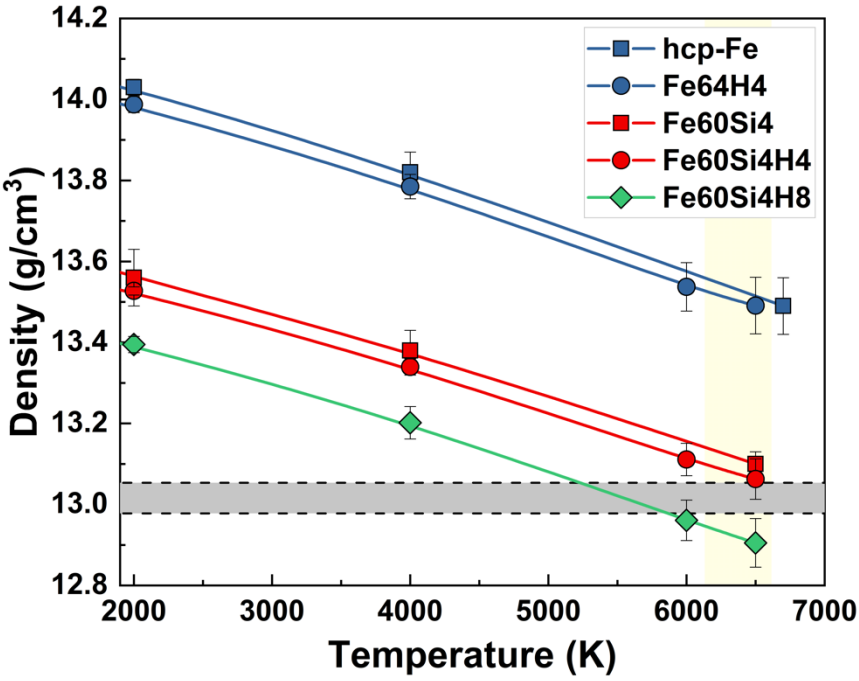

Figure 2. Densities of H-bearing alloys as a function of temperature in comparison with those of *hcp*-Fe and $Fe_{60}Si_4$ at 360 GPa. The grey region enclosed by two dash lines

refers to the observed density range from the PREM and AK135 model (Dziewonski and Anderson, 1981; Kennett et al., 1995). The yellow shaded region represents the possible temperatures at the ICB.

The *hcp*-$Fe_{64}H_4$ is slightly less dense than the *hcp*-Fe, but the difference is not significant when compared with the uncertainty (Fig. 2) due to the low H concentration. Previous studies reported that the incorporation of a substantial amount of H into *hcp*-Fe alloy will decrease its density (Tagawa et al., 2016), consistent with our prediction. Although the V_P and V_S of *hcp*-$Fe_{64}H_4$ are close to the observed values from PREM and AK135 model (Fig. 1), its density is about 2-4% higher than those of seismic models (Fig. 2). Therefore, hydrogen cannot be the sole light element in the Earth's inner core, and some other light elements are required to account for the density.

3.2 Ternary *hcp*-Fe-Si-H alloys

Geochemical evidence suggests that some Si should partition into the Earth's core to account for the super-chondritic Mg/Si ratio and the enrichment of heavy Si isotopes in the bulk silicate Earth relative to chondrites (Georg et al., 2007; Shahar et al., 2009), but its amount has been long debated, varying within several weight percent. Given that the Si partition coefficient between solid and liquid iron is ~1 (Alfè et al., 2002; Zhang et al., 2020), we considered Si as a prime element in the Earth's inner core and have calculated the elastic properties, density, and sound velocities of ternary *hcp*-Fe-Si-H alloys ($Fe_{60}Si_4H_4$ and $Fe_{60}Si_4H_8$) (Fig. 1 and 2).

The MSDs reveal that at temperatures > 4000 K, both *hcp*-$Fe_{60}Si_4H_4$ and $Fe_{60}Si_4H_8$ are also superionic, in which H diffuses rapidly but Fe and Si atoms only slightly oscillate around the equilibrium positions (Fig. S2). As a result, similar to *hcp*-$Fe_{64}H_4$, these two alloys also exhibit a significant shear softening at 6000 K and 6500 K (Fig. 1). Compared with *hcp*-$Fe_{60}Si_4$, *hcp*-$Fe_{60}Si_4H_4$ and $Fe_{60}Si_4H_8$ have similar K_S within the uncertainty but a much lower G at the temperature of the inner core, which result in

a much lower V_S (Fig. 1). For instance, at 6500 K, G and V_S of *hcp*-$Fe_{60}Si_4H_4$ and $Fe_{60}Si_4H_8$ are about 32.0-41.0% and 17.5-22.7% lower than those of *hcp*-$Fe_{60}Si_4$, respectively, while the V_P difference is only ~3.0-4.0%. The *hcp*-$Fe_{60}Si_4H_8$ exhibits relatively lower elastic moduli and sound velocities compared with *hcp*-$Fe_{60}Si_4H_4$ at 6000 K and 6500 K, although the differences are not significant within the uncertainties. In contrast, the density of *hcp*-$Fe_{60}Si_4H_8$ is about 1.5% lower than that of *hcp*-$Fe_{60}Si_4H_4$ (Fig. 2). Our results show that compositions between *hcp*-$Fe_{60}Si_4H_4$ and $Fe_{60}Si_4H_8$ can match the observed seismic velocities and density of the Earth's inner core (Fig. 1 and 2).

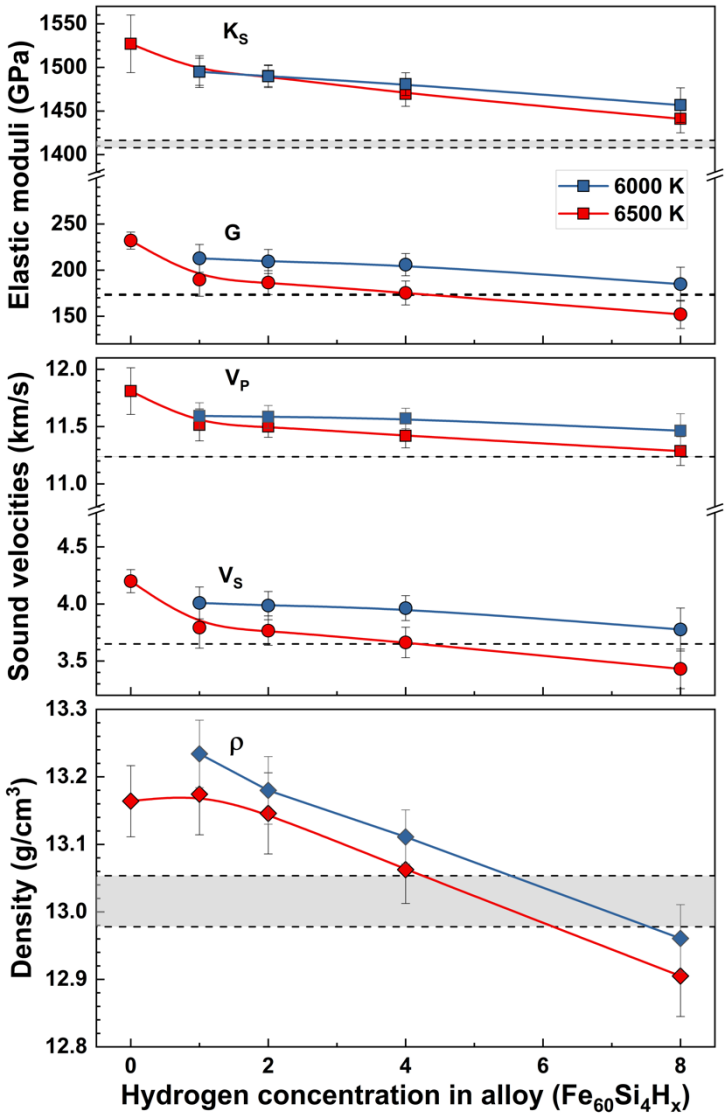

Figure 3. Elastic moduli, sound velocities, and densities of *hcp*-Fe-Si-H alloys ($Fe_{60}Si_4H_x$) as a function of H concentration at 360 GPa. The blue and red points

represent the results at 6000 K and 6500 K, respectively. The results of *hcp*-$Fe_{60}Si_4$ are derived from Martorell et al. (2016). Two dash lines refer to the seismic observations from the PREM and AK135 model (Dziewonski and Anderson, 1981; Kennett et al., 1995).

In order to explore whether other H concentrations can explain the seismic observations, we also conducted simulations on *hcp*-$Fe_{60}Si_4H$ and $Fe_{60}Si_4H_2$ at 6000 K and 6500 K, and similarly, both exhibit superionic behavior (Fig. S3). We find that the elastic moduli, density, and sound velocities of *hcp*-$Fe_{60}Si_4H_x$ generally decrease with H concentration, but the differences between *hcp*-$Fe_{60}Si_4H$, $Fe_{60}Si_4H_2$, and $Fe_{60}Si_4H_4$ are small relative to the uncertainties. However, *hcp*-$Fe_{60}Si_4H_8$ exhibits significantly lower G, density, and V_S than *hcp*-$Fe_{60}Si_4H$ at 6500 K, and the differences exceed the errors (Fig. 3). Thus, one can expect a lower V_S in *hcp*-$Fe_{60}Si_4H_x$ with a higher H concentration ($x > 8$) at 360 GPa and 6500 K, but the incorporation of a large amount of H into the Fe-Si alloy may decrease its melting point and no solid and/or superionic phase may exist under such conditions. When compared to the seismic velocities and density from the PREM and AK135 model, we find that *hcp*-$Fe_{60}Si_4H_2$, $Fe_{60}Si_4H_4$, and $Fe_{60}Si_4H_8$ match the observed V_P, V_S, and density of the inner core within 1.5% simultaneously at 6500 K (Fig. 3). Given that the increase of Si content can somewhat decrease the elastic moduli, density, and sound velocities (Li et al., 2018; Martorell et al., 2016), the *hcp* alloy with Fe:H=60:1 could be also a good candidate for inner core if more Si (Si:Fe>4:60) is incorporated into the alloy. Also, the P-wave anisotropy of *hcp*-Fe-Si-H alloys is 5-8%, which is similar to those of *hcp*-Fe and *hcp*-Fe-Si (Martorell et al., 2016) and sufficient to explain the observed V_P anisotropy in the inner core (summarized in Vočadlo (2015) if the crystals were quite strongly oriented.

Here the temperature of inner core boundary (ICB) is estimated based on the melting curve of Fe from recent shock compression experiments (J. Li et al., 2020; Turneaure et al., 2020) and *ab initio* calculations (Sun et al., 2018). Extensive

experiments were previously conducted to determine the melting points of Fe at high pressures, but large discrepancies in the ICB temperature exist between different studies (Fischer, 2016; Sinmyo et al., 2019), probably because the Fe melt curve beyond 200 GPa remains poorly constrained and different phenomenological criteria were adopted to identify the onset of melting (Anzellini et al., 2013). Recently, Turneaure et al. (2020) conducted *in situ* x-ray diffraction measurements in laser-shock compressed iron along the Hugoniot through shock melting and found that the melt temperature is 5560±360 K at 242 GPa. This value gives an ICB temperature of 6400±360 K, consistent with another recent shock compression study (J. Li et al., 2020) and the results from *ab initio* free energies (Sun et al., 2018). The addition of several weight percentage of Si does not significantly change the melting point of iron (Fischer, 2016) and a small fraction of H could likely only show a weak effect on iron melting (Fukai, 1992). As such, we adopted an ICB temperature of 6000-6500 K in this work. If the ICB temperature is lower than the range we adopted, e.g. ~5500 K, our results with a little extrapolation show that more H (~0.44 wt%, $Fe_{60}Si_4H_{15}$) can also explain the seismic observations of the inner core.

Nomura et al. (2014) suggested a very low ICB temperature (~5000 K), which is an extrapolation based on experiments for melting of wet pyrolite rather than a direct determination of melting of iron alloy. As discussed above, this is not consistent with more recent melting temperature of Fe and its alloys and seems too low. Nevertheless, if we extrapolate our results to 5000 K, an inner core with about 1 wt% H can also match the observed V_S. This amount of H, however, would make the density too low and so at an ICB temperature of 5000 K, H is unlikely to be able to explain V_S, V_P, and density simultaneously with or without another light element.

We did not consider the effect of S on the simulation results. Recent *ab initio* simulations found that the S partition coefficient between the solid and liquid iron phases at core conditions is about 0.75 (Alfè et al., 2002; Zhang et al., 2020), suggesting that S could be an important light element in the inner core. According to the S

abundance in the Earth's mantle (McDonough and Sun, 1995) and the S partition coefficient between metallic and silicate melts during core formation (Rose-Weston et al., 2009), there could be ~1-2 wt% S in the Earth's core and 0.7-1.5 wt% S in the inner core. Li et al. (2018) calculated the elastic moduli and sound velocities of *hcp*-$Fe_{60}Si_4$, $Fe_{60}Si_2S_2$, $Fe_{60}SiS_3$, and $Fe_{60}S_4$ at inner-core conditions and found no significant differences among these Fe-Si-S alloys within the uncertainties. Thus, it can be inferred that the incorporation of S into *hcp*-$Fe_{60}Si_4H_x$ via the S-Si substitution will not significantly affect the density and sound velocities.

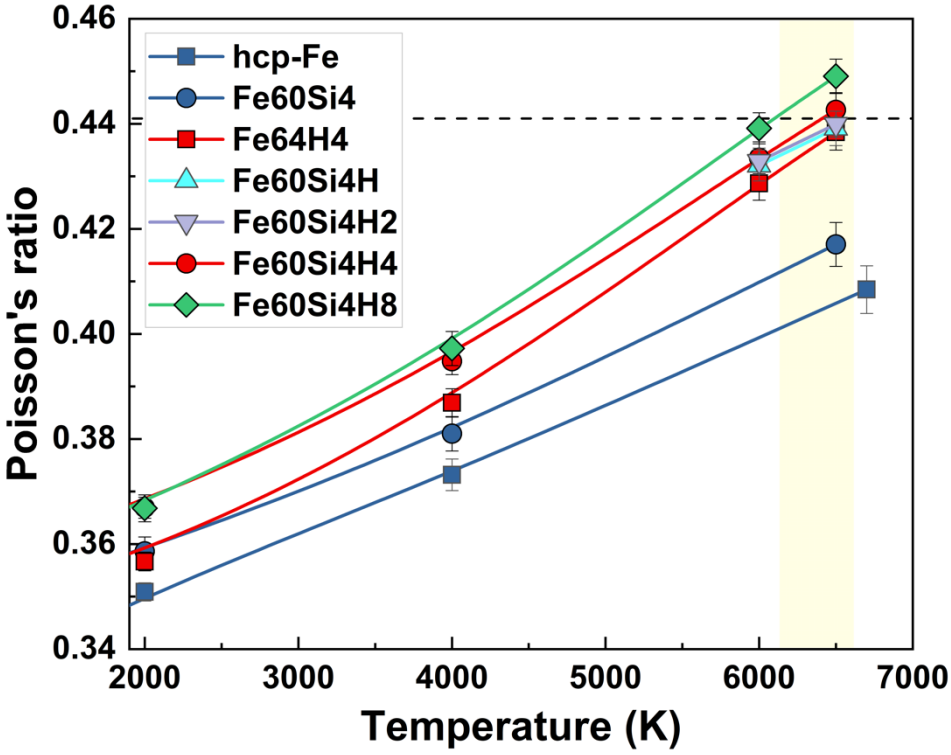

Figure 4. Poisson's ratios of *hcp*-Fe-Si-H alloys ($Fe_{60}Si_4H_x$) as a function of temperature at 360 GPa. The dash line refers to the observed Poisson's ratio from the PREM and AK135 model (Dziewonski and Anderson, 1981; Kennett et al., 1995).

3.3 High Poisson's ratios of *hcp*-Fe-Si-H alloys

Poisson's ratio is derived from the V_P/V_S ratio using the following equation:

$$\nu = \frac{0.5(\frac{V_P}{V_S})^2 - 1}{(\frac{V_P}{V_S})^2 - 1} \quad (4)$$

The results show that the incorporation of H into *hcp*-$Fe_{60}Si_4$ significantly increases its Poisson's ratio and all *hcp*-Fe-Si-H alloys investigated in this study have a high Poisson's ratio (~0.44) at 6500 K that is similar to or larger than the observed value (Fig. 4). This is because the Poisson's ratio is controlled by the K_S/G ratio, and the presence of superionic H in *hcp*-$Fe_{60}Si_4H_x$ alloys leads to a much lower G but a similar K_S compared with *hcp*-$Fe_{60}Si_4$ at inner-core temperature. Some *hcp*-Fe-Si-C alloys and a high-pressure phase of iron carbide Fe_7C_3 were found to also exhibit a Poisson's ratio of 0.44, which is similar to the inner core (Chen et al., 2014; Li et al., 2018, 2016; Prescher et al., 2015), but almost all C preferentially may partition into the liquid iron phase (Li et al., 2019). In contrast, H could partition into the solid iron with the growth of the inner core as solid and liquid iron have a similar local environment of H. Another line of evidence also supports this inference. The diffusion coefficients of H in *hcp*-$Fe_{60}Si_4H_x$ at inner-core conditions (10^{-8}-10^{-7} m^2/s) (Table S2) are similar to those in liquid Fe-H phases (Umemoto and Hirose, 2015), indicating that H atoms freely move between the liquid and solid Fe phases. In summary, the *hcp*-Fe-Si-H alloys can match the observed velocities, density, and the Poisson's ratio in the Earth's inner core simultaneously.

3.4 Implications for hydrogen in the Earth's core

Our results present a strong argument for H as a fundamental light element in the Earth's core (Y. Li et al., 2020), and demonstrate in addition that H alloying can induce a strong shear softening in *hcp*-Fe and *hcp*-Fe-Si at inner-core temperature due to the superionic effect, thus explaining the lower velocities and the high Poisson's ratio in the Earth's inner core. The required H concentration is 0.03-0.23 wt% ($Fe_{60}Si_4H$-$Fe_{60}Si_4H_8$), depending on the inner-core temperature and to what extent mineralogical models and seismic observations need to match in order to be acceptable (Fig. 2 and 3). Such an amount of H corresponds to four to twenty-eight oceans masses of water in the whole core. This assumes that H partitions equally between the liquid and solid Fe

phases, which is supported by the similar H diffusion coefficients in liquid and solid Fe phases (Table S2 and Umemoto and Hirose, 2015). However, it is unlikely that there is about 1 wt% H in the outer core (equal to ~124 oceans of water) (Umemoto and Hirose, 2015), because such an amount of H will cause a much lower inner-core density than the observed value (Fig. 3). Unlike other light elements such as Si and S that can only diffuse in the outer core, H can freely diffuse in both the liquid and solid; such H circulation may play a role in magnetic field generation and sustentation, but such an analysis is outside the scope of this work.

Water could have been segregated from the silicate mantle to the core by mantle-core differentiation due to the large H partition coefficient between the iron and silicate melts (Y. Li et al., 2020) if there was a substantial amount of water dissolved in the silicate mantle during core formation. How and when the water had been accreted into the Earth mainly controls the actual amount of water in the core. It has been argued that Earth's water may come from the late-veneer delivery of water-rich carbonaceous chondrites from beyond the snow line in the solar nebula as they have a D/H (deuterium/ protium) value similar to Earth's oceans (Marty, 2012). In this case, the Earth's core is almost free of water as the proto-Earth accreted little water before or during core formation. However, the deep mantle has a much lower D/H ratio than Earth's oceans, and a solar nebula origin was proposed to account for the depletion of deuterium (Hallis et al., 2015). An early-Earth ingassing model also reveals the capture of nebular hydrogen during Earth's accretion (Olson and Sharp, 2018) and a combination of chondritic water and ingassing of nebular H was further proposed to explain the low D/H value of the Earth (Wu et al., 2018). Recent measurements of enstatite chondrites (EC), which are believed to be representative of the materials that formed Earth (Dauphas, 2017), suggest that they contain sufficient H and have H and N isotopic compositions similar to those of Earth's mantle (Piani et al., 2020). These observations imply that water in the mantle may simply have come from the nebular material from which the planet accreted. Previous studies suggest that at present, the mantle contains

about one ocean of water (Hirschmann, 2018; Wang et al., 2020, 2019). If so, at least four oceans of water should partition into the Earth's core based on a single-stage core-forming process (Y. Li et al., 2020) and this value will be about eight oceans if the one ocean of water at the Earth's surface was also degassed from the mantle during or just after core formation, consistent with our estimate based on the seismic constraints.

Our results support the early delivery of water from chondritic and/or nebular materials before or during core-mantle differentiation. Most water would have been stored in the Earth's core and its D/H ratio dominantly controls the D/H ratio of bulk Earth, and hence it is improper to interpret the origins of Earth's water just from the D/H ratio of the water at the surface and/or in the mantle. Further research on how core formation fractionated the D/H ratio will provide fundamental insight into this unsolved mystery and help to understand the habitability of Earth.

4. Conclusion

We investigated the elastic properties of *hcp*-Fe-H and Fe-Si-H alloys under inner-core conditions using *ab initio* molecular dynamic simulations. We find that in *hcp*-$Fe_{64}H_4$ and all *hcp*-$Fe_{60}Si_4H_x$ (x=1, 2, 4, and 8) investigated in this study, H diffuses rapidly but Fe and Si atoms remain in their equilibrium positions at 6000 K and 6500 K, suggesting that these alloys maintain a superionic state under inner-core conditions. Due to the superionic effect, *hcp*-$Fe_{64}H_4$ and all *hcp*-$Fe_{60}Si_4H_x$ exhibit a strong shear softening at 6000 K and 6500 K, resulting in a much lower V_S. For instance, at 6500 K, G and V_S of *hcp*-$Fe_{64}H_4$ reduce by ~37.6% and 20.9% compared with *hcp*-Fe, respectively, and these properties of *hcp*-$Fe_{60}Si_4H_4$ decrease by ~ 32.0% and 17.5%, respectively. The elastic moduli, density, and sound velocities of *hcp*-$Fe_{60}Si_4H_x$ generally decrease with H concentration, but the differences between *hcp*-$Fe_{60}Si_4H$, $Fe_{60}Si_4H_2$, and $Fe_{60}Si_4H_4$ are small compared to the current uncertainties. However, *hcp*-$Fe_{60}Si_4H_8$ exhibits significantly lower G, density, and V_S than *hcp*-$Fe_{60}Si_4H$ at 6500 K, and the differences exceed the errors. We find that *hcp*-$Fe_{60}Si_4H$, $Fe_{60}Si_4H_2$,

$Fe_{60}Si_4H_4$, and $Fe_{60}Si_4H_8$ can all explain the observed V_P, V_S, and density of the inner core simultaneously. Our results present a strong argument for H as a fundamental light element in the Earth's core, and the required amount of H corresponds to four to twenty-eight oceans of water, consistent with the estimate based on the geochemical constraints. We also support that Earth would have accreted its water from chondritic and/or nebular materials before or during core formation and most water would have partitioned into the core by core-mantle differentiation.

Acknowledgments

W.Z. Wang acknowledges support from the UCL-Carnegie Postdoctoral Scholarship. J.P. Brodholt, L. Vočadlo, and Y. Li acknowledge support from the NERC grant NE/M00046X/1. Y. Li also thank the support from CAS Hundred Talents Program. Z. Wu acknowledges support from the Natural Science Foundation of China (41925017, 41721002). The calculations were conducted partly at the supercomputing center of University of Science and Technology of China.

References

Alfè, D., Gillan, M.J., Price, G.D., 2002. Ab initio chemical potentials of solid and liquid solutions and the chemistry of the Earth's core. J. Chem. Phys. 116, 7127–7136. doi:10.1063/1.1464121

Alfè, D., Kresse, G., Gillan, M.J., 2000. Structure and dynamics of liquid iron under Earth's core conditions. Phys. Rev. B 61, 132–142. doi:10.1103/PhysRevB.61.132

Anderson, W.W., Ahrens, T.J., 1994. An equation of state for liquid iron and implications for the Earth's core. J. Geophys. Res. Solid Earth 99, 4273–4284. doi:10.1029/93JB03158

Antonangeli, D., Siebert, J., Badro, J., Farber, D.L., Fiquet, G., Morard, G., Ryerson, F.J., 2010. Composition of the Earth's inner core from high-pressure sound velocity measurements in Fe–Ni–Si alloys. Earth Planet. Sci. Lett. 295, 292–296. doi:10.1016/j.epsl.2010.04.018

Anzellini, S., Dewaele, A., Mezouar, M., Loubeyre, P., Morard, G., 2013. Melting of Iron at Earth's Inner Core Boundary Based on Fast X-ray Diffraction. Science (80-.). 340, 464–466. doi:10.1126/science.1233514

Badro, J., Cote, A.S., Brodholt, J.P., 2014. A seismologically consistent compositional model of Earth's core. Proc. Natl. Acad. Sci. 111, 7542–7545. doi:10.1073/pnas.1316708111

Bazhanova, Z.G., Oganov, A.R., Gianola, O., 2012. Fe–C and Fe–H systems at pressures of the Earth's inner core. Physics-Uspekhi 55, 489–497. doi:10.3367/UFNe.0182.201205c.0521

Birch, F., 1964. Density and composition of mantle and core. J. Geophys. Res. 69, 4377–4388. doi:10.1029/JZ069i020p04377

Blöchl, P.E., 1994. Projector augmented-wave method. Phys. Rev. B 50, 17953–17979. doi:10.1103/PhysRevB.50.17953

Cavazzoni, C., Chiarotti, G.L., Scandolo, S., Tosatti, E., Bernasconi, M., Parrinello, M., 1999. Superionic and Metallic States of Water and Ammonia at Giant Planet Conditions. Science (80-.). 283, 44–46. doi:10.1126/science.283.5398.44

Chen, B., Li, Z., Zhang, D., Liu, J., Hu, M.Y., Zhao, J., Bi, W., Alp, E.E., Xiao, Y., Chow, P., Li, J., 2014. Hidden carbon in Earth's inner core revealed by shear softening in dense Fe 7 C 3. Proc. Natl. Acad. Sci. 111, 17755–17758. doi:10.1073/pnas.1411154111

Dauphas, N., 2017. The isotopic nature of the Earth's accreting material through time. Nature 541, 521–524. doi:10.1038/nature20830

Dziewonski, A.M., Anderson, D.L., 1981. Preliminary reference Earth model. Phys. Earth Planet. Inter. 25, 297–356. doi:10.1016/0031-9201(81)90046-7

Fischer, R.A., 2016. Melting of Fe Alloys and the Thermal Structure of the Core, in: Deep Earth. pp. 1–12. doi:10.1002/9781118992487.ch1

Fukai, Y., 1992. Some Properties of the Fe-H System at High Pressures and Temperatures, and their Implications for the Earth's Core, in: High-Pressure

Research.' Application to Earth and Planetary Sciences. pp. 373–385. doi:10.1029/GM067p0373
Georg, R.B., Halliday, A.N., Schauble, E. a, Reynolds, B.C., 2007. Silicon in the Earth's core. Nature 447, 1102–1106. doi:10.1038/nature05927
Glatzmaier, G.A., Roberts, P.H., 1996. Rotation and Magnetism of Earth's Inner Core. Science (80-.). 274, 1887–1891. doi:10.1126/science.274.5294.1887
Glatzmaier, G.A., Roberts, P.H., 1995. A three-dimensional self-consistent computer simulation of a geomagnetic field reversal. Nature 377, 203–209. doi:10.1038/377203a0
Hallis, L.J., Huss, G.R., Nagashima, K., Taylor, G.J., Halldórsson, S.A., Hilton, D.R., Mottl, M.J., Meech, K.J., 2015. Evidence for primordial water in Earth's deep mantle. Science (80-.). 350, 795–797. doi:10.1126/science.aac4834
Hill, R., 1952. The Elastic Behaviour of a Crystalline Aggregate. Proc. Phys. Soc. Sect. A 65, 349–354. doi:10.1088/0370-1298/65/5/307
Hirschmann, M.M., 2018. Comparative deep Earth volatile cycles: The case for C recycling from exosphere/mantle fractionation of major (H2O, C, N) volatiles and from H2O/Ce, CO2/Ba, and CO2/Nb exosphere ratios. Earth Planet. Sci. Lett. 502, 262–273. doi:10.1016/j.epsl.2018.08.023
Huang, H., Leng, C., Wang, Q., Young, G., Liu, X., Wu, Y., Xu, F., Fei, Y., 2019. Equation of State for Shocked Fe-8.6 wt% Si up to 240 GPa and 4,670 K. J. Geophys. Res. Solid Earth 124, 8300–8312. doi:10.1029/2019JB017983
Ichikawa, H., Tsuchiya, T., Tange, Y., 2014. The P-V-T equation of state and thermodynamic properties of liquid iron. J. Geophys. Res. Solid Earth 119, 240–252. doi:10.1002/2013JB010732
Kawaguchi, S.I., Nakajima, Y., Hirose, K., Komabayashi, T., Ozawa, H., Tateno, S., Kuwayama, Y., Tsutsui, S., Baron, A.Q.R., 2017. Sound velocity of liquid Fe-Ni-S at high pressure. J. Geophys. Res. Solid Earth 122, 3624–3634. doi:10.1002/2016JB013609
Kennett, B.L.N., Engdahl, E.R., Buland, R., 1995. Constraints on seismic velocities in the Earth from traveltimes. Geophys. J. Int. 122, 108–124. doi:10.1111/j.1365-246X.1995.tb03540.x
Li, J., Fei, Y., 2014. Experimental Constraints on Core Composition, in: Treatise on Geochemistry. Elsevier, pp. 527–557. doi:10.1016/B978-0-08-095975-7.00214-X
Li, J., Wu, Q., Li, Jiabo, Xue, T., Tan, Y., Zhou, X., Zhang, Y., Xiong, Z., Gao, Z., Sekine, T., 2020. Shock Melting Curve of Iron: A Consensus on the Temperature at the Earth's Inner Core Boundary. Geophys. Res. Lett. 47, 1–11. doi:10.1029/2020GL087758
Li, Y., Vočadlo, L., Alfè, D., Brodholt, J., 2019. Carbon Partitioning Between the Earth's Inner and Outer Core. J. Geophys. Res. Solid Earth 124, 12812–12824. doi:10.1029/2019JB018789
Li, Y., Vočadlo, L., Brodholt, J., Wood, I.G., 2016. Thermoelasticity of Fe 7 C 3

under inner core conditions. J. Geophys. Res. Solid Earth 121, 5828–5837. doi:10.1002/2016JB013155
Li, Y., Vočadlo, L., Brodholt, J.P., 2018. The elastic properties of hcp-Fe alloys under the conditions of the Earth's inner core. Earth Planet. Sci. Lett. 493, 118–127. doi:10.1016/j.epsl.2018.04.013
Li, Y., Vočadlo, L., Sun, T., Brodholt, J.P., 2020. The Earth's core as a reservoir of water. Nat. Geosci. 13, 453–458. doi:10.1038/s41561-020-0578-1
Mao, Z., Lin, J.-F., Liu, J., Alatas, A., Gao, L., Zhao, J., Mao, H.-K., 2012. Sound velocities of Fe and Fe-Si alloy in the Earth's core. Proc. Natl. Acad. Sci. 109, 10239–10244. doi:10.1073/pnas.1207086109
Martorell, B., Brodholt, J., Wood, I.G., Vočadlo, L., 2013a. The effect of nickel on the properties of iron at the conditions of Earth's inner core: Ab initio calculations of seismic wave velocities of Fe–Ni alloys. Earth Planet. Sci. Lett. 365, 143–151. doi:10.1016/j.epsl.2013.01.007
Martorell, B., Vocadlo, L., Brodholt, J., Wood, I.G., 2013b. Strong Premelting Effect in the Elastic Properties of hcp-Fe Under Inner-Core Conditions. Science (80-.). 342, 466–468. doi:10.1126/science.1243651
Martorell, B., Wood, I.G., Brodholt, J., Vočadlo, L., 2016. The elastic properties of hcp-Fe 1−x Si x at Earth's inner-core conditions. Earth Planet. Sci. Lett. 451, 89–96. doi:10.1016/j.epsl.2016.07.018
Marty, B., 2012. The origins and concentrations of water, carbon, nitrogen and noble gases on Earth. Earth Planet. Sci. Lett. 313–314, 56–66. doi:10.1016/j.epsl.2011.10.040
McDonough, W.F., Sun, S. -s., 1995. The composition of the Earth. Chem. Geol. 120, 223–253. doi:10.1016/0009-2541(94)00140-4
Millot, M., Coppari, F., Rygg, J.R., Correa Barrios, A., Hamel, S., Swift, D.C., Eggert, J.H., 2019. Nanosecond X-ray diffraction of shock-compressed superionic water ice. Nature 569, 251–255. doi:10.1038/s41586-019-1114-6
Nimmo, F., 2015. Thermal and Compositional Evolution of the Core, in: Treatise on Geophysics. Elsevier, pp. 201–219. doi:10.1016/B978-0-444-53802-4.00160-3
Nomura, R., Hirose, K., Uesugi, K., Ohishi, Y., Tsuchiyama, A., Miyake, A., Ueno, Y., 2014. Low Core-Mantle Boundary Temperature Inferred from the Solidus of Pyrolite. Science (80-.). 343, 522–525. doi:10.1126/science.1248186
Okuchi, T., 1997. Hydrogen Partitioning into Molten Iron at High Pressure: Implications for Earth's Core. Science (80-.). 278, 1781–1784. doi:10.1126/science.278.5344.1781
Olson, P., Sharp, Z.D., 2018. Hydrogen and helium ingassing during terrestrial planet accretion. Earth Planet. Sci. Lett. 498, 418–426. doi:10.1016/j.epsl.2018.07.006
Parrinello, M., Rahman, A., 1980. Crystal Structure and Pair Potentials: A Molecular-Dynamics Study. Phys. Rev. Lett. 45, 1196–1199. doi:10.1103/PhysRevLett.45.1196
Perdew, J.P., Burke, K., Ernzerhof, M., 1996. Generalized Gradient Approximation

Made Simple. Phys. Rev. Lett. 77, 3865–3868. doi:10.1103/PhysRevLett.77.3865
Piani, L., Marrocchi, Y., Rigaudier, T., Vacher, L.G., Thomassin, D., Marty, B., 2020. Earth's water may have been inherited from material similar to enstatite chondrite meteorites. Science (80-.). 369, 1110–1113. doi:10.1126/science.aba1948
Poirier, J.-P., 1994. Light elements in the Earth's outer core: A critical review. Phys. Earth Planet. Inter. 85, 319–337. doi:10.1016/0031-9201(94)90120-1
Prescher, C., Dubrovinsky, L., Bykova, E., Kupenko, I., Glazyrin, K., Kantor, A., McCammon, C., Mookherjee, M., Nakajima, Y., Miyajima, N., Sinmyo, R., Cerantola, V., Dubrovinskaia, N., Prakapenka, V., Rüffer, R., Chumakov, A., Hanfland, M., 2015. High Poisson's ratio of Earth's inner core explained by carbon alloying. Nat. Geosci. 8, 220–223. doi:10.1038/ngeo2370
Rose-Weston, L., Brenan, J.M., Fei, Y., Secco, R.A., Frost, D.J., 2009. Effect of pressure, temperature, and oxygen fugacity on the metal-silicate partitioning of Te, Se, and S: Implications for earth differentiation. Geochim. Cosmochim. Acta 73, 4598–4615. doi:10.1016/j.gca.2009.04.028
Rubie, D.C., Nimmo, F., Melosh, H.J., 2015. Formation of the Earth's Core, in: Treatise on Geophysics. Elsevier, pp. 43–79. doi:10.1016/B978-0-444-53802-4.00154-8
Shahar, A., Ziegler, K., Young, E.D., Ricolleau, A., Schauble, E.A., Fei, Y., 2009. Experimentally determined Si isotope fractionation between silicate and Fe metal and implications for Earth's core formation. Earth Planet. Sci. Lett. 288, 228–234. doi:10.1016/j.epsl.2009.09.025
Singh, S.C., Taylor, M.A., Montagner, J.P., 2000. On the Presence of Liquid in Earth's Inner Core. Science (80-.). 287, 2471–2474. doi:10.1126/science.287.5462.2471
Sinmyo, R., Hirose, K., Ohishi, Y., 2019. Melting curve of iron to 290 GPa determined in a resistance-heated diamond-anvil cell. Earth Planet. Sci. Lett. 510, 45–52. doi:10.1016/j.epsl.2019.01.006
Sun, T., Brodholt, J.P., Li, Y., Vočadlo, L., 2018. Melting properties from ab initio free energy calculations: Iron at the Earth's inner-core boundary. Phys. Rev. B 98, 224301. doi:10.1103/PhysRevB.98.224301
Tagawa, S., Ohta, K., Hirose, K., Kato, C., Ohishi, Y., 2016. Compression of Fe-Si-H alloys to core pressures. Geophys. Res. Lett. 43, 3686–3692. doi:10.1002/2016GL068848
Turneaure, S.J., Sharma, S.M., Gupta, Y.M., 2020. Crystal Structure and Melting of Fe Shock Compressed to 273 GPa: In Situ X-Ray Diffraction. Phys. Rev. Lett. 125, 215702. doi:10.1103/PhysRevLett.125.215702
Umemoto, K., Hirose, K., 2015. Liquid iron-hydrogen alloys at outer core conditions by first-principles calculations. Geophys. Res. Lett. 42, 7513–7520. doi:10.1002/2015GL065899

Vočadlo, L., 2015. Earth's Core: Iron and Iron Alloys, in: Treatise on Geophysics. Elsevier, pp. 117–147. doi:10.1016/B978-0-444-53802-4.00032-4

Vočadlo, L., 2007. Ab initio calculations of the elasticity of iron and iron alloys at inner core conditions: Evidence for a partially molten inner core? Earth Planet. Sci. Lett. 254, 227–232. doi:10.1016/j.epsl.2006.09.046

Vočadlo, L., Alfè, D., Gillan, M.., Price, G.D., 2003. The properties of iron under core conditions from first principles calculations. Phys. Earth Planet. Inter. 140, 101–125. doi:10.1016/j.pepi.2003.08.001

Vočadlo, L., Dobson, D.P., Wood, I.G., 2009. Ab initio calculations of the elasticity of hcp-Fe as a function of temperature at inner-core pressure. Earth Planet. Sci. Lett. 288, 534–538. doi:10.1016/j.epsl.2009.10.015

Wang, W., Walter, M.J., Peng, Y., Redfern, S., Wu, Z., 2019. Constraining olivine abundance and water content of the mantle at the 410-km discontinuity from the elasticity of olivine and wadsleyite. Earth Planet. Sci. Lett. 519, 1–11. doi:10.1016/j.epsl.2019.04.018

Wang, W., Zhang, H., Brodholt, J.P., Wu, Z., 2020. Elasticity of hydrous ringwoodite at mantle conditions: Implication for water distribution in the lowermost mantle transition zone. Earth Planet. Sci. Lett. 554, 116626. doi:10.1016/j.epsl.2020.116626

Wood, B.J., Walter, M.J., Wade, J., 2006. Accretion of the Earth and segregation of its core. Nature 441, 825–833. doi:10.1038/nature04763

Wu, J., Desch, S.J., Schaefer, L., Elkins-Tanton, L.T., Pahlevan, K., Buseck, P.R., 2018. Origin of Earth's Water: Chondritic Inheritance Plus Nebular Ingassing and Storage of Hydrogen in the Core. J. Geophys. Res. Planets 123, 2691–2712. doi:10.1029/2018JE005698

Zhang, Z., Csányi, G., Alfè, D., 2020. Partitioning of sulfur between solid and liquid iron under Earth's core conditions: Constraints from atomistic simulations with machine learning potentials. Geochim. Cosmochim. Acta 291, 5–18. doi:10.1016/j.gca.2020.03.028